4 January 2002

Chemical Physics Letters 351 (2002) 27–34

CHEMICAL PHYSICS LETTERS

www.elsevier.com/locate/cplett

Raman studies on 0.4 nm diameter single wall carbon nanotubes

A. Jorio [a,*], A.G. Souza Filho [a,d], G. Dresselhaus [b], M.S. Dresselhaus [a,c], A. Righi [e], F.M. Matinaga [e], M.S.S. Dantas [e], M.A. Pimenta [e], J. Mendes Filho [d], Z.M. Li [f], Z.K. Tang [f], R. Saito [g]

[a] *Department of Physics, Massachusetts Institute of Technology, 77 Massachusetts Ave., Room 13-3005, Cambridge, MA 02139-4307, USA*

[b] *Francis Bitter Magnet Laboratory, Massachusetts Institute of Technology, 77 Massachusetts Ave., Room 13-3005, Cambridge, MA 02139-4307, USA*

[c] *Department of Electrical Engineering and Computer Science, Massachusetts Institute of Technology, 77 Massachusetts Ave., Room 13-3005, Cambridge, MA 02139-4307, USA*

[d] *Departamento de Física, Universidade Federal do Ceará, Fortaleza, CE 60455-760, Brazil*

[e] *Departamento de Física, Universidade Federal de Minas Gerais, Belo Horizonte, MG 30123-970, Brazil*

[f] *Physics Department, Hong Kong University of Science and Technology, Clear Water Bay, Kowloon, Hong Kong*

[g] *Department of Electronic-Engineering, University of Electro-Communications, Tokyo 182-8585, Japan*

Received 4 September 2001

Abstract

We performed polarized Raman scattering studies on 0.4 nm diameter single wall carbon nanotubes (SWNTs) grown inside the pores of zeolite crystals, using several different laser lines ($1.92 \leqslant E_{laser} \leqslant 2.71$ eV). The strong diameter-selective resonant behavior of typical SWNTs ($1 < d_t < 3$ nm) is not observed. The Raman spectra instead show a complicated profile that reflects the sp^2 carbons phonon density of states superimposed on the characteristic SWNT Raman features. We show that the behavior of typical SWNTs can be used qualitatively to analyze the radial breathing mode (RBM), *G*-band and *D*-band spectra of the 0.4 nm diameter SWNTs.

1. Introduction

Carbon nanotubes have been extensively studied recently due to their unusual physical properties [1,2]. Because of their one-dimensional (1D) character, single wall carbon nanotubes (SWNTs) exhibit quantum confinement in their electronic structure, and they can be either metallic or semiconducting depending on their geometry [2]. Recently, very small diameter SWNTs were fabricated inside the channels of $AlPO_4$-5 (AFI) zeolite single crystals [3,4]. Imaging simulations of high-resolution transmission electron microscopy (HRTEM) observations indicate that the SWNTs

* Corresponding author. Fax: +1-617-253-6827.
E-mail address: adojorio@mgm.mit.edu (A. Jorio).

0009-2614/02/$ - see front matter
PII: S0009-2614(01)01336-7

formed in the AFI crystals measure just 4.2 ± 0.2 Å in diameter (d_t) [5], consistent with the size of the pores in the AFI crystal (inner diameter 7.3 Å) after subtracting twice the van der Waals radius (~1.7 Å). Therefore, these SWNTs have the same d_t as the smallest possible fullerene C_{20}, that is formed by just 12 pentagons. Noteworthy is the recent report of superconductivity below $T_c = 15$ K in these small d_t SWNTs [6].

Only three different SWNTs can be formed inside the small zeolite channels: the metallic $(5,0)$ and $(3,3)$, and the semiconducting $(4,2)$ SWNTs. Although the band-folding scheme and tight binding calculations imply that the $(5,0)$ SWNT should be semiconducting, ab initio calculations show that the large curvature in such a small d_t SWNT leads to a hybridization of the σ^* and π^* orbitals, and the Fermi level becomes populated. These SWNTs have been characterized also by diffuse X-ray scattering [7], polarized optical absorption [8], and polarized micro-Raman measurements [4,9,10], and the complementary results indicate that SWNTs with $d_t \sim 0.4$ nm are indeed present in the AFI channels. We here present a systematic resonant Raman study of the SWNT + AFI sample using several different laser lines. We show that the complicated experimental Raman profile from 100 to 1700 cm^{-1} reflects the phonon density of states (PDOS) of sp^2 carbons [11], some features typical of the 1D PDOS for the (n,m) SWNTs present in the sample, as well as their radial breathing mode (RBM), *G*-band and *D*-band features.

2. Experimental details

Samples of SWNTs ~0.4 nm in diameter are grown by pyrolyzing tripropylamine (TPA) in the channels of the zeolite crystals $AlPO_4$-5 (AFI) [4]. Polarized micro-Raman back-scattering experiments were performed using an ArKr laser on a pure AFI sample containing TPA *before* SWNT formation (TPA + AFI), and in different samples *after* SWNT formation (SWNT + AFI), including a visually defective SWNT + AFI sample. Different polarization scattering geometries were obtained by rotating the sample/analyzer. Several different laser lines were used: $E_{laser} = 1.92$, 1.95, 2.18, 2.34, 2.38, 2.41, 2.54 and 2.71 eV. A DILOR XY triple-monochromator equipped with a N_2 cooled charged coupled device (CCD) was used to acquire the spectra.

3. Results

Fig. 1(a) shows the general spectra obtained with three different laser lines, with both the incident and scattered light polarized parallel to the nanotube axes [(ZZ) configuration]. The Raman peaks appear over a broad luminescence band, and both the Raman and fluorescence intensities depend on E_{laser}. Fig. 1(b) shows spectra obtained with $E_{laser} = 2.41$ eV in the (ZZ), (ZX) and (XX) scattering geometries, showing that both the Raman and fluorescence signals are strongly suppressed for light polarized perpendicular to Z, consistent with the depolarization or antenna effect observed in typical SWNTs, where absorption and emission are strongly suppressed for light polarized perpendicular to the nanotube axes [8,12–14]. No fluorescence is observed in the spectra of the pure AFI sample with TPA before

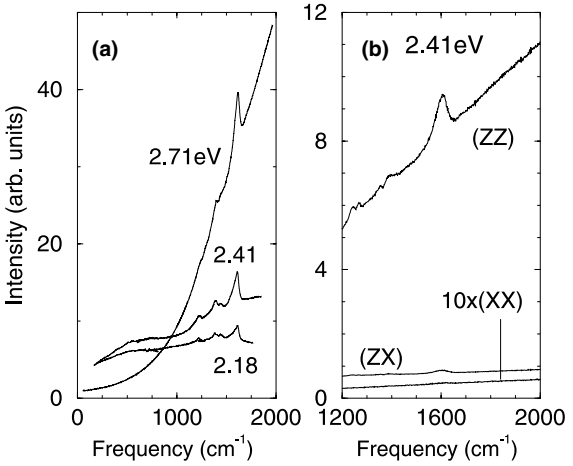

Fig. 1. (a) General spectra of a SWNT + AFI sample for $E_{laser} = 2.18$, 2.41 and 2.71 eV, in the (ZZ) scattering geometry. Z is the nanotube axis direction and Y is the laser propagation direction. (b) SWNT + AFI spectra obtained with $E_{laser} = 2.41$ eV in the (ZZ), (ZX) and (XX) scattering geometries. The (XX) spectrum was multiplied by 10.

SWNT formation (TPA + AFI). The intensity behaviors of the Raman and fluorescence signals are consistent with earlier optical absorption experiments, that show a smooth increase in absorption from 1.6 up to 4.1 eV [8].

The Raman spectra of the sample are shown in the region of the radial breathing modes (RBM) in Fig. 2(a) and in the region of the *G*-band modes in Fig. 2(b) for different E_{laser} values, obtained after suppressing the broad fluorescent background. The spectra at the bottom of Fig. 2(a) and (b) come from a TPA + AFI sample using $E_{\text{laser}} = 1.92$ eV. All the other spectra were obtained from a SWNT + AFI sample. We observed some variation in the relative mode intensities from spectra acquired with different $E_{\text{laser lines}}$, but such a variation is also observed when measuring different spots on the sample with the same E_{laser}. In general, the same spectral features are observed in all the SWNT + AFI spectra.

Measurements on SWNTs with a typical diameter size ($\sim 1 < d_t < \sim 3$ nm), either in bundles [15] or as isolated tubes [16–18], show a strong diameter-selective resonance Raman process, the Raman signal being strongly enhanced when E_{laser} matches an electronic transition E_{ii} between 1D van Hove singularities in the valence and conducting bands. The Raman spectra from $\sim$0.4 nm d_t SWNTs do exhibit an E_{laser}-dependent intensity and antenna effect, that is related to the resonant nature of the scattering process. However, the spectra do not seem to exhibit a clear diameter-selective resonance Raman behavior as is observed for typical SWNTs. This result might be related to the relatively large energy dispersion of the electron branches in the 1D Brillouin zone (BZ) [8].

As shown in Fig. 2, the Raman spectra of these 0.4 nm d_t SWNTs in their AFI templates exhibit a complicated profile. These data can be understood by comparing the general Raman spectra of the SWNT + AFI sample with the PDOS in two-dimensional (2D) graphite and in SWNTs. Fig. 3 shows the Raman spectra of a SWNT + AFI sample obtained with $E_{\text{laser}} = 2.41$ eV in the (ZZ) scattering geometry, after subtracting the fluorescence background. The lower curves show the calculated PDOS in 2D graphite [11] and the sum of the calculated PDOS for the $(5,0)$, $(3,3)$ and

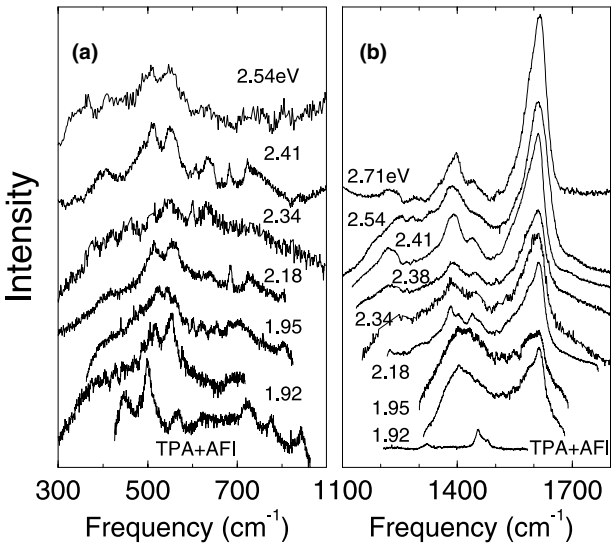

Fig. 2. Raman spectra of the sample in the region of (a) the RBMs and (b) the *G*-band modes for different E_{laser}, obtained after suppressing the broad fluorescent background (see Fig. 1). The spectra in the bottom of (a) and (b) come from a TPA + AFI sample using $E_{\text{laser}} = 1.92$ eV. The other spectra were obtained from a SWNT + AFI sample. Some points were deleted from the spectra obtained with $E_{\text{laser}} = 2.34$ eV due to the appearance of plasma lines. No features appear in the 300–900 cm^{-1} spectra for $E_{\text{laser}} = 2.38$ and 2.71 eV, which are therefore not shown.

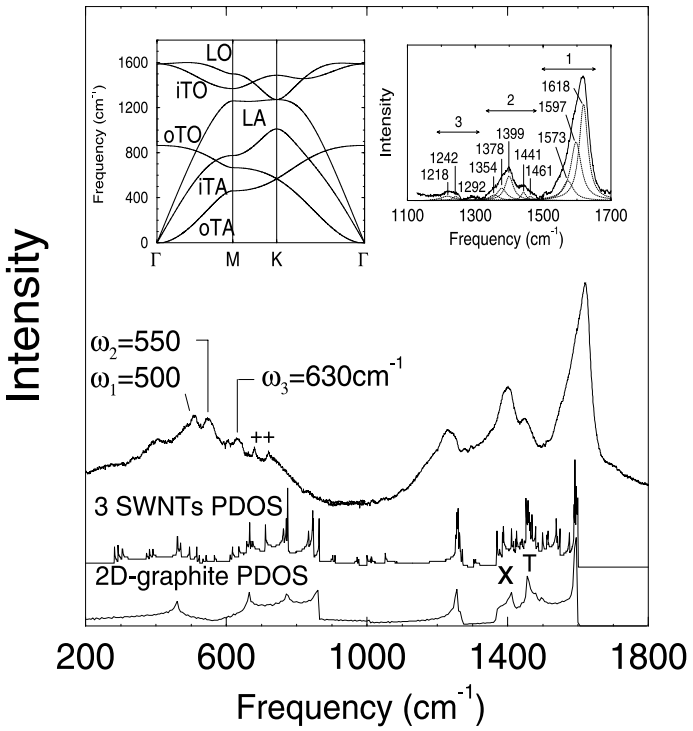

Fig. 3. From top to bottom: Raman spectra of a SWNT + AFI sample obtained with $E_{laser} = 2.41$ eV in the (ZZ) scattering geometry after subtracting the fluorescence background; sum of the PDOS for the $(5,0)$, $(3,3)$ and $(4,2)$ SWNTs; PDOS for 2D graphite. The '++', 'X' and 'T' symbols indicate features discussed in the text. The left inset shows the phonon dispersion of 2D graphite [11]. The right inset shows a Lorentzian fit to the spectrum obtained with $E_{laser} = 2.71$ eV in the 1100–1700 cm^{-1} region. The various modes are grouped into the frequency regions denoted by 1, 2 and 3. The frequencies of the Lorentzian peaks are in cm^{-1}.

$(4,2)$ SWNTs (see Fig. 4). The SWNT PDOS was calculated in Fig. 4 by the tight-binding molecular dynamics method [2,19]. The Raman signal and the PDOS show a surprising similarity, especially above 1200 cm^{-1}. Some significant differences are also observed and, as we discuss below, these features are related to the RBMs and the *G*-band modes that appear due to the circumferential boundary conditions in SWNTs [2].

Above 1000 cm^{-1}, the experimental spectrum in Fig. 3 can be divided into three different regions (see right inset to Fig. 3) as follows: (1) the highest frequency and strongest peaks between 1500 and 1650 cm^{-1}; (2) the modes between 1310 and 1480 cm^{-1}; (3) the modes between 1200 and 1300 cm^{-1}. All the spectra obtained with different E_{laser} values exhibit this general behavior (see Fig. 2), which is also in agreement with previous micro-Raman studies on 0.4 nm d_t SWNTs using $E_{laser} = 1.96$ eV [4,9,10]. To analyze these frequency regions in more detail, we select the spectrum at $E_{laser} = 2.71$ eV and fit the main features in each region with Lorentzian lineshapes (see right inset to Fig. 3).

Region (1) in the right inset to Fig. 3 exhibits a strong Raman peak at 1618 cm^{-1}, identified with the maximum in the graphite PDOS that is common to all SWNTs (see Figs. 3 and 4) and is related to a flat region in the highest LO 2D graphite phonon branch away from the Γ point (see left inset to Fig. 3). The 1597 cm^{-1} Raman peak has no equivalent feature in the PDOS and we relate this feature to the *G*-band in SWNTs [15]. The 1573 cm^{-1} Raman peak can be assigned to a peak in the PDOS that appears for the $(3,3)$ and $(4,2)$ SWNTs (see '$*$' in Fig. 4), and is not a 2D graphite

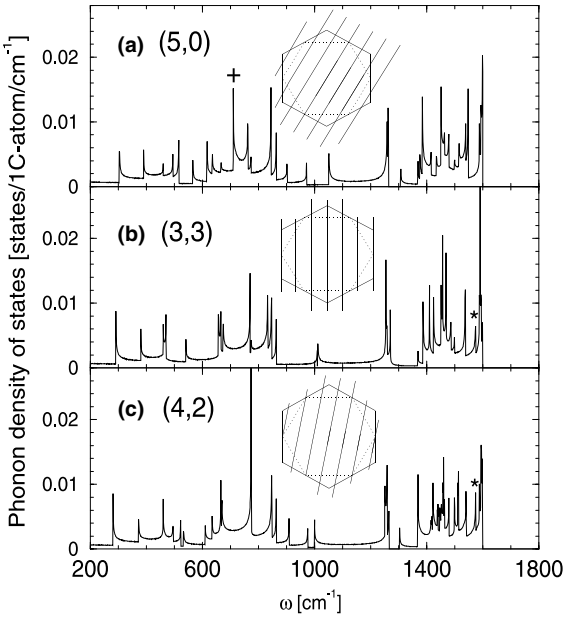

Fig. 4. PDOS for the (a) $(5,0)$, (b) $(3,3)$, and (c) $(4,2)$ SWNTs calculated by a tight-binding molecular dynamics method [2,19]. The '$*$' and '+' symbols indicate PDOS peaks discussed in the text. The insets show the cutting lines of the 1D SWNT Brillouin zone (BZ) on the 2D graphite BZ for the three SWNTs.

feature. The $(5,5)$ SWNT does not exhibit such a peak in its PDOS. The differences in the PDOS for the different (n,m) SWNTs can be understood considering that, although the $(5,0)$, $(3,3)$ and $(4,2)$ SWNTs have similar d_t values, the different nanotube chiralities θ change the PDOS significantly, due to the differences in the resulting cutting lines of the 1D SWNT Brillouin zone with the 2D graphite Brillouin zone (see insets to Fig. 4). For example, in the case of the $(5,0)$ and $(4,2)$ SWNTs, the cutting lines cross the M point, while for the $(3,3)$ armchair SWNT, the cutting lines cross the K point and there is then no trigonal warping effect [2].

Region (2) exhibits two Raman peaks, 1441 and 1461 cm^{-1}, that can be directly assigned to a feature in both the 2D graphite and SWNT PDOS (see 'T' in Fig. 3). This PDOS feature comes from two flat regions in the 2D graphite phonon dispersion, one in the LO mode branch at the M point, and another in the in-plane TO (iTO) mode branch in the Γ–K direction. The stronger Raman feature observed between 1354 and 1399 cm^{-1} has a contribution from the flat region in the iTO mode branch at the M point of 2D graphite (see 'X' in Fig. 3). However, this feature generally exhibits a larger intensity than would be expected from the PDOS, appearing even when the peaks at 1441 and 1461 cm^{-1} have very low intensity. As we discuss below, this band also has contributions from the G-band of the SWNTs.

The tangential G-band modes in nanotubes can exhibit vibrations along the tube axis direction (G^+ mode) or along the circumferential direction (G^- modes). These modes are split due to zone folding and nanotube curvature [20–24], and the G^-/G^+ splitting depends on d_t [21,22]. By measuring isolated $1 < d_t < 3$ nm SWNTs [21], the frequency ω_{G^-} of the second most intense peak in the spectrum was found to depend strongly on d_t through the simple relation $\omega_{G^-} = \omega_{G^+} - C/d_t^2$, with $C = 45.8$ cm^{-1} nm^2 for semiconducting SWNTs and $C = 79.5$ cm^{-1} nm^2 for metallic SWNTs [21]. Metallic SWNTs show an additional downshift, presumably, due to phonon–plasmon coupling [25].

In [21], ω_{G^+} was always found to be close to 1591 cm^{-1}, independent of d_t. Using this result for guidance, we identify the G^+-band peak for the 0.4 nm d_t SWNTs with the feature at 1597 cm^{-1}. The model $\omega_{G^-} = \omega_{G^+} - C/d_t^2$ yields, for $d_t = 0.4$ nm, $\omega_{G^-} = 1312$ cm^{-1} for semiconducting SWNTs and $\omega_{G^+} = 1069$ cm^{-1} for metallic SWNTs. Although the $(5,0)$ and $(3,3)$ SWNTs are all predicted to be metallic, the ω_{G^-} prediction for semiconducting SWNTs (1305 cm^{-1}) provides a better estimate for the observed peak frequency for the lower A symmetry G^--band mode occurring around 1370 cm^{-1}. The additional ω_{G^-} downshift expected for $1 < d_t < 3$ nm metallic SWNTs is due to a Breit–Wigner–Fano (BWF) coupling. However, the BWF peak requires a discrete level in the continuum spectra [25], but no phonon with frequency around 1069 cm^{-1} can appear near the Γ point. We note that the strong BWF lineshape generally found for metallic SWNTs [15] is not observed for the 0.4 nm d_t SWNTs. Therefore, the feature fits by three Lorentzian peaks at 1354, 1378 and 1399 cm^{-1} observed in region (2) are related

both to peaks in the SWNT PDOS (see Fig. 4) and to G^--band modes from SWNTs inside the AFI channels.

Region (3) clearly comes from the feature in the PDOS (see Fig. 3) that is related to flat regions in the LO 2D graphite phonon branch at the K point, and in the LA 2D graphite phonon branch in the M-K region. Fig. 4 shows that in SWNTs this feature occurs around 1250 cm^{-1}, corresponding to the frequency region (3). The small peak at 1292 cm^{-1} also comes from the LO 2D graphite phonon branch and a peak is observed at $\sim$1305 cm^{-1} in the PDOS of the $(5,0)$ and $(4,2)$ SWNTs (see Figs. 3 and 4).

Phonon modes not at the Γ point ($q = 0$) are generally observed in the case of disordered materials and they are dispersive in E_{laser}. The LO phonon branch in 2D graphite close to the K point is responsible for the well-known D-band in sp^2 materials, that is a strongly dispersive band, for which the frequency ω_D shows a strong linear dependence on E_{laser} [26–29]. Previous works show that ω_D in SWNTs decreases with decreasing d_t, and has a $1/d_t$ dependence for $1 < d_t < 3$ nm [30,31]. Considering $d_t = 0.4$ nm, we extrapolate $\omega_D = 1314$ cm^{-1}, which is quite close to the small peak at 1292 cm^{-1} observed in region (3).

In general, the peak frequencies obtained in the present Raman experiment appear to be about 10–30 cm^{-1} lower than both the calculated frequency values for the 1D SWNT PDOS peaks (see Figs. 3 and 4) and for the extrapolated frequency behavior from the $1 < d_t < 3$ nm SWNTs [21,31]. This result gives us a measure of sp^2–sp^3 mixing of the atomic bonds that are responsible for a general softening of the phonon frequencies, and this mixing occurs because of the large curvature in 0.4 nm d_t SWNTs.

When one probes phonons in the interior of the graphite Brillouin zone, one expects to observe a dispersive behavior for the mode frequencies by varying E_{laser}. This dispersive behavior is modified in SWNTs due to the electron and phonon quantization along the circumferential direction [29,31,32]. Fig. 5 shows two spectra obtained at $E_{laser} = 1.92$ and 2.41 eV but at different places of a defective SWNT + AFI sample. For some spots, strong features are observed in the $\sim$1250 cm^{-1} region (3), and at other laser spots, these features are absent. Comparing the strong peaks in the upper spectra for $E_{laser} = 1.92$ and 2.41 eV, we can identify a dispersive behavior that appears to occur by an intensity transfer between discrete phonon lines. This behavior is better illustrated in the inset to Fig. 5, which shows spectra in region (3), obtained with three different laser lines: $E_{laser} = 2.18$ (a), 2.41 (b), and 2.54 eV (c). By increasing E_{laser}, the three peaks at 1220, 1239 and 1268 cm^{-1} interchange intensity. The 1220 cm^{-1} peak is strongest for $E_{laser} = 2.18$ eV, while the 1239 cm^{-1} peak is strongest for $E_{laser} = 2.54$ eV. The identification of these features with the D band gives $\Delta\omega = 53$ cm^{-1} eV^{-1}, in excellent agreement with the general dispersive behavior observed for the disorder-induced D-band in SWNT bundles [29]. However, we emphasize that the spectra change for different samples probed with the same E_{laser}, as can be seen by comparing the $E_{laser} = 2.41$ eV D-band spectra observed in

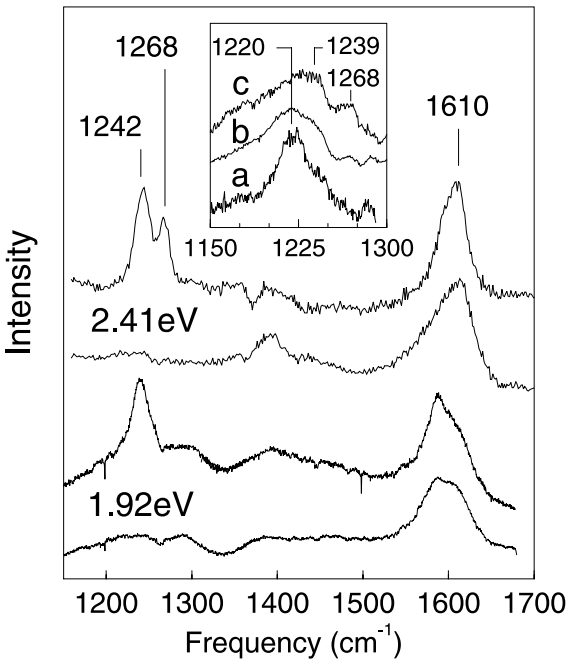

Fig. 5. Raman spectra in the region of the G- and D-bands obtained with $E_{laser} = 1.92$ and 2.41 eV, at different laser spots on a SWNT + AFI sample. The inset shows the D-band spectra obtained with three different laser lines: E_{laser} = (a) 2.18, (b) 2.41, and (c) 2.54 eV.

Fig. 5 and in the inset to Fig. 5. More detailed studies are necessary to characterize the quantum nature of the *D*-band dispersive behavior for the 0.4 nm d_t SWNTs.

Between 900 and 1100 cm^{-1} no Raman scattering is observed experimentally, in agreement with the small magnitude of the PDOS (see Fig. 3). Below 900 cm^{-1} the PDOS increases and we observe Raman scattering again. The strong features in the PDOS between 600 and 900 cm^{-1} are identified with branches of non-Raman active out-of-plane TO (oTO) and in-plane TA (iTA) phonon branches (see left inset to Fig. 3), suggesting that the scattering is disorder-induced. For this frequency region, the agreement between the Raman spectra and the PDOS profile is not as good as that observed above 1200 cm^{-1}, and this is because the PDOS features above 1200 cm^{-1} come from a branch of the Raman-active E_{2g} mode. However, the experimental observation of two sharp peaks at 680 and 720 cm^{-1} (see '++' in Fig. 3) are particularly noteworthy. The 680 cm^{-1} peak is identified with a 2D graphite-like peak in the PDOS that is also present in SWNTs, while the 720 cm^{-1} peak is identified with a singularity in the PDOS of the $(5,0)$ SWNT (see '+' in Fig. 4) that is not present in 2D graphite.

The strong Raman intensity observed at about 540 cm^{-1} has no equivalent in the PDOS. In previous polarized Raman studies, the 540 cm^{-1} feature was assigned to the RBM [4,9,10]. Resonant Raman spectra on isolated SWNTs [16] gives the relation $\omega_{RBM} = 248/d_t$. This relation yields $\omega_{RBM} = 590$, 600, and 625 cm^{-1} for the $(4,2)$, $(3,3)$, and $(5,0)$ SWNTs, respectively. In Fig. 3 we observe three strong peaks at $\omega_1 = 500$, $\omega_2 = 550$, and $\omega_3 = 630$ cm^{-1}. Qualitatively, these peaks appear in an appropriate frequency region for the RBM features, and ω_2 and ω_3 are further away from each other, compared to ω_1 and ω_2, as is also found for the theoretical values. Thus, we tentatively identify ω_1, ω_2, and ω_3 with the RBMs for $(4,2)$, $(3,3)$, and $(5,0)$ SWNTs, respectively.

Finally, the peaks observed in the 1D SWNT PDOS below ~400 cm^{-1} are identified with the 2D graphite acoustic modes (see Figs. 3 and 4). In Fig. 3, we can see peaks around 300 and 400 cm^{-1} which should correspond to acoustic modes. The peaks around 450 cm^{-1} observed in the PDOS of both SWNTs and 2D graphite (see Figs. 3 and 4) are singularities related to the flat dispersion of the out-of-plane TA (oTA) mode close to the 2D graphite *M* point. Such types of features are also found in other sp^2 graphite materials, where their appearance is explained by a double resonance process [33].

4. Summary and conclusion

In summary, we performed Raman scattering studies on 0.4 nm d_t SWNTs grown inside the channels of zeolite crystals, using several different laser lines. The spectra show a broad luminescence that exhibits a E_{laser} dependence and polarization behavior similar to the resonant Raman signal from the SWNTs. The strong diameter-selective resonant behavior characteristic of $1 < d_t < 3$ nm SWNTs is not observed for the 0.4 nm d_t SWNTs in the AFI channels, probably due to the strong energy dispersion of the electronic bands.

The Raman spectra show a complicated profile that reflects the SWNTs PDOS superimposed on the characteristic SWNT Raman features, namely, the RBM, the *G*-band and *D*-band features. The fact that the PDOS profile is observed in the Raman spectra suggests that disorder plays an important role in the Raman scattering of the 0.4 nm d_t SWNTs. We show that the behavior for the commonly studied $1 < d_t < 3$ nm SWNTs can be used qualitatively to assign the frequencies of the vibrational modes in these 0.4 nm diameter SWNTs, including the RBM and *G*-band modes. Especially noteworthy is the appearance of Raman features related to peaks that appears only in the 1D SWNT PDOS. We also observe dispersive modes in connection with the ~1250 cm^{-1} feature, related to the *D*-band behavior in typical sp^2 carbon materials. Dispersive Raman features at lower frequencies are related to the acoustic branches.

Acknowledgements

Experiments were performed in the micro-Raman laboratory, Universidade Federal de Minas

Gerais, Brazil, supported by FAPEMIG, CNPq and FINEP. A.J./A.G.S.F./A.R. acknowledge financial support from the Brazilian agencies CNPq/CAPES/FAPEMIG. Z.K.T. acknowledges RGC Grant (No. HKUST6149/01P) from Research Grants Council of Hong Kong. R.S. acknowledges a Grant-in-Aid (No. 13440091) from the Ministry of Education, Japan. The MIT authors acknowledge support under NSF Grants DMR 01-16042, INT 98-15744 and INT 00-00408. We acknowledge the NSF/CNP_q joint collaboration program that makes possible exchange trips between MIT and UFMG researchers (No. NSF INT 00-00408 and No. CNP_q 910120/99-4).

References

[1] M.S. Dresselhaus, P. Avouris, Carbon Nanotubes: Synthesis, Structure, Properties and Applications, Topics in Applied Physics, Springer, Berlin, 2001.
[2] R. Saito, G. Dresselhaus, M.S. Dresselhaus, Physical Properties of Carbon Nanotubes, Imperial College Press, London, 1998.
[3] N. Wang, Z.K. Tang, G.D. Li, J.S. Chen, Nature 408 (2000) 50.
[4] Z.K. Tang, H.D. Sun, J. Wang, J. Chen, G. Li, Appl. Phys. Lett. 73 (1998) 2287.
[5] N. Wang, G.D. Li, Z.K. Tang, Chem. Phys. Lett. 339 (2001) 47.
[6] Z.K. Tang, L. Zhang, N. Wang, X.X. Zhang, G.H. Wen, G.D. Li, J.N. Wang, C.T. Chan, P. Sheng, Science 292 (2001) 2462.
[7] P. Launois, R. Moret, D. Le Bolloc'h, P.A. Albouy, Z.K. Tang, G. Li, J. Chen, Solid State Commun. 116 (2000) 99.
[8] Z.M. Li, Z.K. Tang, H.J. Liu, N. Wang, C.T. Chan, R. Saito, S. Okada, G.D. Li, J.S. Chen, Phys. Rev. Lett. 87 (2001) 127401.
[9] H.D. Sun, Z.K. Tang, J. Chen, G. Li, Solid State Commun. 109 (1999) 365.
[10] Z.K. Tang, H.D. Sun, J. Wang, Physica B 279 (2000) 200.
[11] P. Lespade, R. Al-Jishi, M.S. Dresselhaus, Carbon 20 (1982) 427.
[12] H. Ajiki, T. Ando, Physica B 201 (1994) 349.
[13] G.S. Duesberg, I. Loa, M. Burghard, K. Syassen, S. Roth, Phys. Rev. Lett. 85 (2000) 5436.
[14] A. Jorio, A.G. Souza Filho, V.W. Brar, A.K. Swan, M.S. Ünlü, B.B. Goldberg, A. Righi, J.H. Hafner, C.M. Lieber, R. Saito, G. Dresselhaus, M.S. Dresselhaus, Phys. Rev. B (2001), BGR859 (submitted).
[15] M.S. Dresselhaus, P.C. Eklund, Adv. Phys. 49 (2000) 705.
[16] A. Jorio, R. Saito, J.H. Hafner, C.M. Lieber, M. Hunter, T. McClure, G. Dresselhaus, M.S. Dresselhaus, Phys. Rev. Lett. 86 (2001) 1118.
[17] A. Jorio, A.G. Souza Filho, G. Dresselhaus, M.S. Dresselhaus, R. Saito, J.H. Hafner, C.M. Lieber, F.M. Matinaga, M.S.S. Dantas, M.A. Pimenta, Phys. Rev. B 63 (2001) 245416.
[18] A.G. Souza Filho, A. Jorio, J.H. Hafner, C.M. Lieber, R. Saito, M.A. Pimenta, G. Dresselhaus, M.S. Dresselhaus, Phys. Rev. B 63 (2001) 241404R.
[19] R. Saito, T. Takeya, T. Kimura, G. Dresselhaus, M.S. Dresselhaus, Phys. Rev. B 57 (1998) 4145.
[20] R. Saito, A. Jorio, J.H. Hafner, C.M. Lieber, M. Hunter, T. McClure, G. Dresselhaus, M.S. Dresselhaus, Phys. Rev. B 64 (2001) 085312.
[21] A. Jorio, A.G. Souza Filho, G. Dresselhaus, M.S. Dresselhaus, A.K. Swan, B. Goldberg, M.S. Ünlü, M.A. Pimenta, J.H. Hafner, C.M. Lieber, R. Saito, Phys. Rev. B (2001), BF8180 (submitted).
[22] A. Kasuya, Y. Sasaki, Y. Saito, K. Tohji, Y. Nishina, Phys. Rev. Lett. 78 (1997) 4434.
[23] A. Jorio, G. Dresselhaus, M.S. Dresselhaus, M. Souza, M.S.S. Dantas, M.A. Pimenta, A.M. Rao, R. Saito, C. Liu, H.M. Cheng, Phys. Rev. Lett. 85 (2000) 2617.
[24] L. Alvarez, A. Righi, S. Rols, E. Englaret, J.L. Sauvajol, E. Munoz, W.R. Moser, A.M. Benito, M.T. Martínes, G.F. de la Fuente, Phys. Rev. B 63 (2001) 153401.
[25] S.D.M. Brown, A. Jorio, P. Corio, M.S. Dresselhaus, G. Dresselhaus, R. Saito, K. Kneipp, Phys. Rev. B 63 (2001) 5414.
[26] F. Tuinstra, J.L. Koenig, J. Chem. Phys. 53 (1970) 1126.
[27] R.P. Vidano, D.B. Fishbach, L.J. Willis, T.M. Loehr, Solid State Commun. 39 (1981) 341.
[28] M.J. Matthews, M.A. Pimenta, S.D.M. Brown, A. Marucci, M.S. Dresselhaus, M. Endo, C. Kim, in: M. Endo (Ed.), Extended Abstract for the International Symposium on Carbon Science and Technology for New Carbons, Tokyo, November 8–12, 1998.
[29] M.A. Pimenta, E.B. Hanlon, A. Marucci, P. Corio, S.D.M. Brown, S.A. Empedocles, M.G. Bawendi, G. Dresselhaus, M.S. Dresselhaus, Braz. J. Phys. 30 (2000) 423.
[30] M.A. Pimenta, A. Jorio, S.D.M. Brown, A.G. Souza Filho, G. Dresselhaus, J.H. Hafner, C.M. Lieber, R. Saito, M.S. Dresselhaus, Phys. Rev. B 64 (2001) 041401.
[31] A.G. Souza Filho, A. Jorio, G. Dresselhaus, M.S. Dresselhaus, A.K. Swan, M.S. Ünlü, B.B. Goldberg, R. Saito, J.H. Hafner, C.M. Lieber, M.A. Pimenta, Phys. Rev. B (2001) (in press).
[32] A.G. Souza Filho, A. Jorio, G. Dresselhaus, M.S. Dresselhaus, R. Saito, A.K. Swan, B.B. Goldberg, M.S. Ünlü, J.H. Hafner, C.M. Lieber, M.A. Pimenta, Phys. Rev. B (2001), BE8318 (submitted).
[33] R. Saito, A. Jorio, A.G. Souza Filho, G. Dresselhaus, M.S. Dresselhaus, M.A. Pimenta, Phys. Rev. Lett. (2001), LH8274 (in press).